Proceedings of the 40th IEEE
Conference on Decision and Control
Orlando, Florida USA, December 2001

Visual Servoing Based on Intersample Disturbance Rejection by Multirate Sampling Control

– Time Delay Compensation and Experimental Verification –

Hiroshi Fujimoto† and Yoichi Hori‡

†Department of Electrical Engineering, Nagaoka University of Technology, Japan
‡Department of Electrical Engineering, The University of Tokyo, Japan
fujimoto@vos.nagaokaut.ac.jp, hori@hori.t.u-tokyo.ac.jp

Abstract

In this paper, novel multirate sampling controllers are proposed for digital control systems, where the speed of the A/D converters is restricted to be slower than that of the D/A converters. The proposed feedback controller assures perfect disturbance rejection (PDR) at M intersample points in the steady state. The proposed method is extended to systems with time delay, and the compensation method is proposed based on the observer including time delay model. Next, the novel scheme of repetitive control is proposed based on the open-loop estimation and switching function, which enables the rejection of periodical disturbance without any sacrifice of the closed-loop characteristics. Finally, the proposed controllers are applied to visual servo system by introducing the workspace controller and nonlinear perspective transformation. The advantages of these approaches are demonstrated by simulations and experiments using a robot manipulator.

1 Introduction

A generalized digital control system is shown in Fig. 1, where $P_c(s)$ is a continuous-time plant to be controlled, $\boldsymbol{C}[z]$ is a discrete-time controller implemented in digital computer. Because the discrete-time controller has to deal with continuous-time signals, it needs to have two samplers $\mathcal{S}$ for the reference signal $r(t)$ and the output $y(t)$, and one holder $\mathcal{H}$ on the input $u(t)$. Therefore, there exist three time periods T_r, T_y, and T_u which represent the periods of $r(t), y(t)$, and $u(t)$, respectively. The input period T_u is generally decided by the speed of the actuator, D/A converter, or the calculation on the CPU. The output period T_y is also determined by the speed of the sensor or the A/D converter.

Actual control systems usually hold hardware restrictions on these periods (T_u and/or T_y). Moreover, in case of multivariable systems, there exist many time periods. However, the conventional digital control systems often make all periods equal to the longest period for simplification. On the other hand, the multirate sampling control systems have been studied from the point of view both of control theories and practical applications [1, 2].

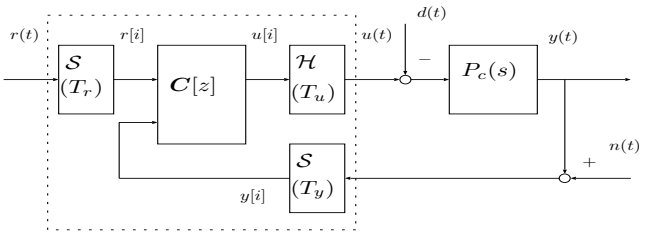

Figure 1: Digital control system.

Authors have developed a novel multirate feedforward controller, in which the control input is changed several times during T_r [3, 4]. In this paper, new multirate feedback controller is considered. Historically, many multirate feedback control theories have been developed as surveyed in [1]. These theoretical approaches have reached the negative result that feedback characteristics such as disturbance rejection performance and stability robustness are never improved by the multirate control [5, 6].

However, this theoretical result is limited to the case where there is no hardware restriction on the sampling scheme ($T_y = T_u$). On the other hand, many industrial systems have hardware restrictions in their sampling mechanisms. Thus, in this paper, digital control systems where the sampling periods of plant output are longer than the control periods ($T_u < T_y$) are considered. For these systems, novel multirate feedback controller is proposed which improves intersample disturbance rejection performance.

The restriction of $T_u < T_y$ may be general because D/A converters are usually faster than the A/D converters. In particular, head-positioning systems of hard disk drives [4] and visual servo systems of robot manipulators belong to this category, because the sampling rates of the measurement are relatively slow. In this paper, the proposed controllers are applied to the visual servo system, and the advantages are verified through simulations and experiments using a robot manipulator.

0-7803-7061-9/01/$10.00 © 2001 IEEE

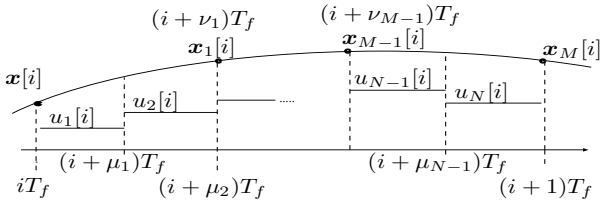

Figure 2: Multirate sampling control.

2 Perfect Disturbance Rejection Control

For the restriction of $T_u < T_y$, the frame period T_f is defined as $T_f = T_y$, and the dynamics of the controller is described by T_f [1]. For simplification, the continuous-time plant is assumed to be a SISO system in this paper. The proposed methods, however, can be extended to deal with the MIMO system [2, 7].

In the proposed multirate scheme, the plant input is changed N times during T_f and the plant state is evaluated M times in this interval, as shown in Fig. 2. The positive integers M and N are referred to as input and state multiplicities, respectively. N is determined by the hardware restriction, and M is defined as $M = N/n$, where n is the plant order.

In Fig. 2, $\mu_j (j = 0, 1, \cdots, N)$ and $\nu_k (k = 1, \cdots, M)$ are parameters for the timing of input changing and state evaluation, which satisfy the following conditions.

$$0 = \mu_0 < \mu_1 < \mu_2 < ... < \mu_N = 1 \tag{1}$$

$$0 < \nu_1 < \nu_2 < ... < \nu_M = 1 \tag{2}$$

If T_y is divided at equal intervals, the parameters are set to $\mu_j = j/N$ and $\nu_k = k/M$.

2.1 Plant Discretization by Multirate Sampling

Consider the continuous-time plant described by

$$\dot{\boldsymbol{x}}(t) = \boldsymbol{A_c}\boldsymbol{x}(t) + \boldsymbol{b_c}u(t)\ , \quad y(t) = \boldsymbol{c}_c\boldsymbol{x}(t). \tag{3}$$

The discrete-time plant discretized by the multirate sampling control of Fig. 2 becomes

$$\boldsymbol{x}[i+1] = \boldsymbol{A}\boldsymbol{x}[i] + \boldsymbol{B}\boldsymbol{u}[i]\ , \quad y[i] = \boldsymbol{C}\boldsymbol{x}[i], \tag{4}$$

where $\boldsymbol{x}[i] = \boldsymbol{x}(iT)$, and where matrices $\boldsymbol{A}, \boldsymbol{B}, \boldsymbol{C}$, and vector $\boldsymbol{u}[i]$ are given by

$$\left[\begin{array}{c|c} \boldsymbol{A} & \boldsymbol{B} \\ \hline \boldsymbol{C} & \boldsymbol{O} \end{array}\right] := \left[\begin{array}{c|ccc} e^{\boldsymbol{A_c}T_f} & \boldsymbol{b}_1 & \cdots & \boldsymbol{b}_N \\ \hline \boldsymbol{c}_c & 0 & \cdots & 0 \end{array}\right], \tag{5}$$

$$\boldsymbol{b}_j := \int_{(1-\mu_j)T_f}^{(1-\mu_{(j-1)})T_f} e^{\boldsymbol{A_c}\tau}\boldsymbol{b_c}d\tau\ ,\ \boldsymbol{u}[i] := [u_1[i], \cdots, u_N[i]]^T. \tag{6}$$

The intersample plant state at $t = (i + \nu_k)T_f$ is represented by

$$\tilde{\boldsymbol{x}}[i] = \tilde{\boldsymbol{A}}\boldsymbol{x}[i] + \tilde{\boldsymbol{B}}\boldsymbol{u}[i], \tag{7}$$

where $\tilde{\boldsymbol{x}}[i]$ is a vector composed of the intersample plant state $\boldsymbol{x}_k[i] := \boldsymbol{x}((i + \nu_k)T_f)$ [1].

$$\begin{aligned} \tilde{\boldsymbol{x}}[i] &:= [\boldsymbol{x}_1^T[i], \cdots, \boldsymbol{x}_M^T[i]]^T \\ &= [\boldsymbol{x}_1^T((i+\nu_1)T_f), \cdots, \boldsymbol{x}_M^T((i+1)T_f)]^T \end{aligned} \tag{8}$$

[1]The operation of (8) is called "discrete-time lifting" in advanced sampled-data control theory [8] .

The coefficient matrices of (7) are given by

$$\left[\ \tilde{\boldsymbol{A}}\ \middle|\ \tilde{\boldsymbol{B}}\ \right] := \left[\begin{array}{c|ccc} \tilde{\boldsymbol{A}}_1 & \tilde{\boldsymbol{b}}_{11} & \cdots & \tilde{\boldsymbol{b}}_{1N} \\ \vdots & \vdots & & \vdots \\ \tilde{\boldsymbol{A}}_M & \tilde{\boldsymbol{b}}_{M1} & \cdots & \tilde{\boldsymbol{b}}_{MN} \end{array}\right], \tag{9}$$

$$\tilde{\boldsymbol{A}}_k := e^{\boldsymbol{A_c}\nu_k T_f}, \tag{10}$$

$$\tilde{\boldsymbol{b}}_{kj} := \left\{\begin{array}{cc} \mu_j < \nu_k : & \int_{(\nu_k-\mu_j)T_f}^{(\nu_k-\mu_{(j-1)})T_f} e^{\boldsymbol{A_c}\tau}\boldsymbol{b_c}d\tau \\ \mu_{(j-1)} < \nu_k \le \mu_j : & \int_0^{(\nu_k-\mu_{(j-1)})T_f} e^{\boldsymbol{A_c}\tau}\boldsymbol{b_c}d\tau \\ \nu_k \le \mu_{(j-1)} : & 0 \end{array}\right. .$$

2.2 Design of Perfect Disturbance Rejection Controller

In this section, a new multirate feedback controller is proposed based on the state-space design method of disturbance observer.

Consider the continuous-time plant described by

$$\dot{\boldsymbol{x}}_p(t) = \boldsymbol{A}_{cp}\boldsymbol{x}_p(t) + \boldsymbol{b}_{cp}(u(t) - d(t)) \tag{11}$$

$$y(t) = \boldsymbol{c}_{cp}\boldsymbol{x}_p(t), \tag{12}$$

where $d(t)$ is the disturbance input. Let the disturbance model be

$$\dot{\boldsymbol{x}}_d(t) = \boldsymbol{A}_{cd}\boldsymbol{x}_d(t),\ d(t) = \boldsymbol{c}_{cd}\boldsymbol{x}_d(t). \tag{13}$$

For example, the step type disturbance can be modeled by $\boldsymbol{A}_{cd} = 0, \boldsymbol{c}_{cd} = 1$, and sinusoidal type disturbance with frequency ω_d can be modeled by

$$\boldsymbol{A}_{cd} = \left[\begin{array}{cc} 0 & 1 \\ -\omega_d^2 & 0 \end{array}\right],\ \ \boldsymbol{c}_{cd} = [1, 0]. \tag{14}$$

The continuous-time augmented system consisting of (11) and (13) is represented by

$$\dot{\boldsymbol{x}}(t) = \boldsymbol{A}_c\boldsymbol{x}(t) + \boldsymbol{b}_c u(t) \tag{15}$$

$$y(t) = \boldsymbol{c}_c\boldsymbol{x}(t) \tag{16}$$

$$\boldsymbol{A}_c := \left[\begin{array}{cc} \boldsymbol{A}_{cp} & -\boldsymbol{b}_{cp}\boldsymbol{c}_{cd} \\ \boldsymbol{O} & \boldsymbol{A}_{cd} \end{array}\right], \boldsymbol{b}_c := \left[\begin{array}{c} \boldsymbol{b}_{cp} \\ \boldsymbol{0} \end{array}\right], \boldsymbol{x} := \left[\begin{array}{c} \boldsymbol{x}_p \\ \boldsymbol{x}_d \end{array}\right],$$
$$\boldsymbol{c}_c := [\boldsymbol{c}_{cp}, \boldsymbol{0}].$$

Discretizing (15) using multirate sampling control, the intersample plant state at $t = (i + \nu_k)T_f$ can be calculated from the kth row of (7) as

$$\boldsymbol{x}[i + \nu_k] = \tilde{\boldsymbol{A}}_k\boldsymbol{x}[i] + \tilde{\boldsymbol{B}}_k\boldsymbol{u}[i] \tag{17}$$

$$\tilde{\boldsymbol{A}}_k = \left[\begin{array}{cc} \tilde{\boldsymbol{A}}_{pk} & \tilde{\boldsymbol{A}}_{pdk} \\ \boldsymbol{O} & \tilde{\boldsymbol{A}}_{dk} \end{array}\right], \tilde{\boldsymbol{B}}_k = \left[\begin{array}{c} \tilde{\boldsymbol{B}}_{pk} \\ \boldsymbol{O} \end{array}\right].$$

For the plant discretized by (4) from (15), the discrete-time observer at the sampling points is obtained from Gopinath's method by

$$\hat{\boldsymbol{v}}[i+1] = \hat{\boldsymbol{A}}\hat{\boldsymbol{v}}[i] + \hat{\boldsymbol{b}}y[i] + \hat{\boldsymbol{J}}\boldsymbol{u}[i] \tag{18}$$

$$\hat{\boldsymbol{x}}[i] = \hat{\boldsymbol{C}}\hat{\boldsymbol{v}}[i] + \hat{\boldsymbol{d}}y[i]. \tag{19}$$

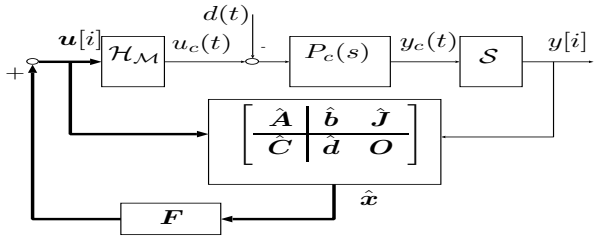

Figure 3: Multirate control with disturbance observer.

As shown in Fig. 3, let the feedback control law be

$$\boldsymbol{u}[i] = \boldsymbol{u}_p[i] + \boldsymbol{u}_d[i] = \boldsymbol{F}_p\hat{\boldsymbol{x}}_p[i] + \boldsymbol{F}_d\hat{\boldsymbol{x}}_d[i] = \boldsymbol{F}\hat{\boldsymbol{x}}[i], \quad (20)$$

where $\boldsymbol{F} := [\boldsymbol{F}_p, \boldsymbol{F}_d]$. Letting $\boldsymbol{e}_v[i]$ be the estimation error of the observer ($\boldsymbol{e}_v[i] = \hat{\boldsymbol{v}}[i] - \boldsymbol{v}[i]$), the following equation is obtained.

$$\hat{\boldsymbol{x}}[i] = \boldsymbol{x}[i] + \hat{\boldsymbol{C}}\boldsymbol{e}_v[i]. \quad (21)$$

From (17) to (21), the closed-loop system is represented by

$$\left[\begin{array}{c} \boldsymbol{x}_p[i+\nu_k] \\ \boldsymbol{x}_d[i+\nu_k] \\ \boldsymbol{e}_v[i+1] \end{array}\right] = \left[\begin{array}{ccc} \tilde{\boldsymbol{A}}_{pk} + \tilde{\boldsymbol{B}}_{pk}\boldsymbol{F}_p & \tilde{\boldsymbol{A}}_{pdk} + \tilde{\boldsymbol{B}}_{pk}\boldsymbol{F}_d & \tilde{\boldsymbol{B}}_{pk}\boldsymbol{F}\hat{\boldsymbol{C}} \\ \boldsymbol{O} & \tilde{\boldsymbol{A}}_{dk} & \boldsymbol{O} \\ \boldsymbol{O} & \boldsymbol{O} & \hat{\boldsymbol{A}} \end{array}\right] \left[\begin{array}{c} \boldsymbol{x}_p[i] \\ \boldsymbol{x}_d[i] \\ \boldsymbol{e}_v[i] \end{array}\right]. \quad (22)$$

Because full row rank of the matrix $\tilde{\boldsymbol{B}}_{pk}$ can be assured by [9], $\boldsymbol{F}_d$ can be selected such that the (1,2) element of the above equation becomes zero for all $k = 1, \cdots, M$.

$$\tilde{\boldsymbol{A}}_{pdk} + \tilde{\boldsymbol{B}}_{pk}\boldsymbol{F}_d = \boldsymbol{O} \quad (23)$$

The simultaneous equation of (23) for all k becomes

$$\tilde{\boldsymbol{A}}_{pd} + \tilde{\boldsymbol{B}}_p\boldsymbol{F}_d = \boldsymbol{O}, \quad (24)$$

$$\left[\begin{array}{c|c} \tilde{\boldsymbol{A}}_{pd} & \tilde{\boldsymbol{B}}_p \end{array}\right] := \left[\begin{array}{c|c} \tilde{\boldsymbol{A}}_{pd1} & \tilde{\boldsymbol{B}}_{p1} \\ \vdots & \vdots \\ \tilde{\boldsymbol{A}}_{pdM} & \tilde{\boldsymbol{B}}_{pM} \end{array}\right]. \quad (25)$$

From (24), $\boldsymbol{F}_d$ is obtained by

$$\boldsymbol{F}_d = -\tilde{\boldsymbol{B}}_p^{-1}\tilde{\boldsymbol{A}}_{pd}. \quad (26)$$

In (22) and (23), the influence from disturbance $\boldsymbol{x}_d[i]$ to the intersample state $\boldsymbol{x}_p[i+\nu_k]$ at $t = (i+\nu_k)T_f$ can become zero. Moreover, $\boldsymbol{x}_p[i]$ and $\boldsymbol{e}_v[i]$ at the sampling point converge to zero at the rate of the eigenvalues of $\tilde{\boldsymbol{A}}_{pM} + \tilde{\boldsymbol{B}}_{pM}\boldsymbol{F}_p$ and $\hat{\boldsymbol{A}}$ (the poles of the regulator and observer). Therefore, perfect disturbance rejection is achieved ($\boldsymbol{x}_p[i+\nu_k] = 0$) in the steady state. The poles of the regulator and observer will be tuned by taking account of the tradeoff between the performance and stability robustness. In [4], the gain $\boldsymbol{F}_p$ is designed using intersample observer, which enables to increase the stability margin by compensating large delay generated by holder.

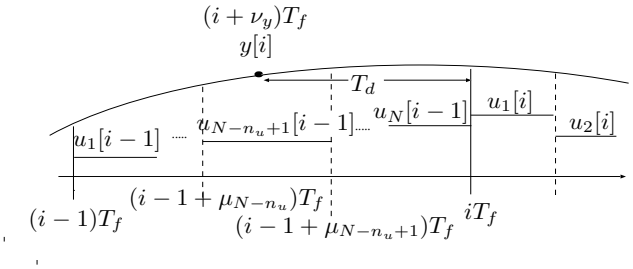

Figure 4: Time chart of the time delay.

Substituting (18) for (20), the feedback type controller is obtained by

$$\left[\begin{array}{c} \hat{\boldsymbol{v}}[i+1] \\ \boldsymbol{u}[i] \end{array}\right] = \left[\begin{array}{cc} \hat{\boldsymbol{A}} + \hat{\boldsymbol{J}}\boldsymbol{F}\hat{\boldsymbol{C}} & \hat{\boldsymbol{b}} + \hat{\boldsymbol{J}}\boldsymbol{F}\hat{\boldsymbol{d}} \\ \boldsymbol{F}\hat{\boldsymbol{C}} & \boldsymbol{F}\hat{\boldsymbol{d}} \end{array}\right] \left[\begin{array}{c} \hat{\boldsymbol{v}}[i] \\ y[i] \end{array}\right]. \quad (27)$$

In this paper, the state multiplicity is defined as $M = N/n$ in order to reject the disturbance perfectly at M inter-sample points. On the other hand, M was selected more than N/n to optimize the inter-sample performance in [10].

2.3 Extension to Systems with Time Delay

In this section, the proposed multirate feedback control is extended to plants with time delay. The continuous-time plant with time delay T_d is described by

$$\dot{\boldsymbol{x}}(t) = \boldsymbol{A}_c\boldsymbol{x}(t) + \boldsymbol{b}_c u(t) \quad (28)$$

$$y(t) = \boldsymbol{c}_c\boldsymbol{x}(t - T_d), \quad (29)$$

as shown in Fig. 4. Because the time delay is considered to be generated by the output signal processing or calculation, it is assumed to be shorter than the frame period ($T_d \le T_f$) for simplification. However, longer time delay can also be considered in the same way as [11].

The discrete-time plant with multirate hold can be represented by

$$\bar{\boldsymbol{x}}[i+1] = \bar{\boldsymbol{A}}\bar{\boldsymbol{x}}[i] + \bar{\boldsymbol{B}}\boldsymbol{u}[i] \quad (30)$$

$$\bar{\boldsymbol{y}}[i] = \bar{\boldsymbol{C}}\bar{\boldsymbol{x}}[i] \quad (31)$$

$$\bar{\boldsymbol{A}} := \left[\begin{array}{cc} \boldsymbol{A} & \boldsymbol{O} \\ \boldsymbol{O} & \boldsymbol{O} \end{array}\right], \ \bar{\boldsymbol{B}} := \left[\begin{array}{c} \boldsymbol{B} \\ \boldsymbol{E} \end{array}\right], \ \bar{\boldsymbol{C}} := \left[\begin{array}{cc} \boldsymbol{c} & \boldsymbol{g} \\ \boldsymbol{O} & \boldsymbol{I}_{n_u} \end{array}\right],$$

$$\bar{\boldsymbol{x}} := \left[\begin{array}{c} \boldsymbol{x} \\ \boldsymbol{x}_u \end{array}\right], \ \bar{\boldsymbol{y}} := \left[\begin{array}{c} y \\ \boldsymbol{x}_u \end{array}\right] \quad (32)$$

$$\boldsymbol{c} := \boldsymbol{c}_c e^{\boldsymbol{A}_c\nu_y T_f}, \boldsymbol{g} := [g_{N-n_u+1}, \cdots, g_N], \quad (33)$$

$$g_j := \begin{cases} \nu_y \le -1 + \mu_{(j-1)} : \\ \qquad -\boldsymbol{c}_c e^{\boldsymbol{A}_c\nu_y T_f}\int_{(1-\mu_j)T_f}^{(1-\mu_{(j-1)})T_f} e^{\boldsymbol{A}_c\tau}\boldsymbol{b}_c d\tau \\ -1 + \mu_{(j-1)} \le \nu_y < -1 + \mu_j : \\ \qquad -\boldsymbol{c}_c e^{\boldsymbol{A}_c\nu_y T_f}\int_{(1-\mu_j)T_f}^{-\nu_y T_f} e^{\boldsymbol{A}_c\tau}\boldsymbol{b}_c d\tau \\ -1 + \mu_j \le \nu_y < 0 : \qquad 0 \end{cases},$$

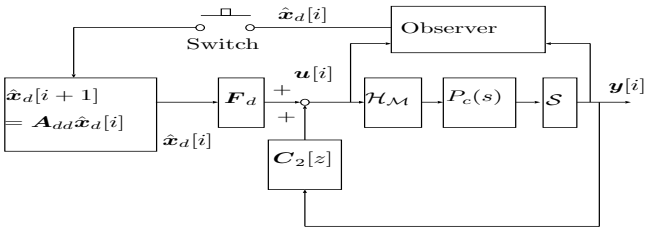

Figure 5: Feedforward repetitive control.

$$\boldsymbol{E} := [\boldsymbol{O}, \boldsymbol{I}_{n_u}], \nu_y := -\frac{T_d}{T_f} \tag{34}$$

where n_u is a number of $\boldsymbol{u}[i-1]$ elements during T_d in Fig. 4, and $\boldsymbol{x}_u$ is a vector composed of this control input ($\boldsymbol{x}_u[i] = [u_{N-n_u+1}[i-1], \cdots, u_N[i-1]]^T$). In (31), the measurement variable $\bar{\boldsymbol{y}}$ includes the past control input $\boldsymbol{x}_u$ in order to make the system observable.

For the plant with time delay represented by (30) and (31), the discrete-time observer at the sampling points is obtained. Thus, using the feedback gain designed in (26), let the control law be

$$\boldsymbol{u}[i] = \bar{\boldsymbol{F}}\bar{\boldsymbol{x}}[i], \quad \bar{\boldsymbol{F}} := [\boldsymbol{F}_d, \boldsymbol{O}]. \tag{35}$$

By the parallel discussion with section 2.2, perfect disturbance rejection performance is preserved by (35).

3 Periodic Disturbance Rejection Control

In this section, perfect disturbance rejection control is applied to periodic disturbance, and two multirate repetitive controllers are proposed [10], they are 1) feedback approach based on the internal model principle and 2) feedforward disturbance rejection approach based on open-loop estimation.

3.1 Feedback Repetitive Control

The disturbance with period $T_0 := 2\pi/\omega_0$ can be represented by the Fourier series as

$$d(t) = a_0 + \sum_{k=1}^{\infty} a_k \cos k\omega_0 t + b_k \sin k\omega_0 t. \tag{36}$$

where ω_0 is known and a_k, b_k are unknown parameters. Letting the disturbance model (13) be (36), the repetitive feedback controller is obtained by (27), including the internal model $s^2 + (k\omega_0)^2$ in discrete-time domain. Repetitive disturbance is perfectly rejected ($\boldsymbol{x}_p[i+\nu_k] = 0$) at M inter-sample points in the steady state.

3.2 Feedforward Repetitive Control

Repetitive feedback control based on the internal model principle has disadvantages that closed-loop characteristics worsen and it becomes difficult to assure stability robustness [12]. Therefore, in this section, a novel repetitive controller based on open-loop estimation with switching function and feedforward disturbance rejection is proposed, as shown in Fig. 5

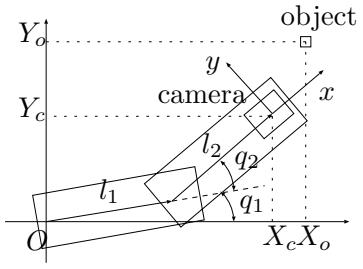

Figure 6: Two-link DD robot with camera.

The repetitive disturbance is estimated by the open-loop disturbance observer. When the estimation converges to the steady state, the switch turns on at $t = t_0$. After that, the switch turns off immediately. Repetitive disturbance is calculated by (37) from the initial value $\hat{\boldsymbol{x}}_d[t_0]$ which contains the amplitude and phase information of the disturbance.

$$\hat{\boldsymbol{x}}_d[i+1] = \boldsymbol{A}_{dd}\hat{\boldsymbol{x}}_d[i], \quad \boldsymbol{A}_{dd} = e^{\boldsymbol{A}_{cd}T_f} \tag{37}$$

Because the disturbance feedforward $\boldsymbol{F}_d$ is obtained by (26), perfect disturbance rejection is achieved at M inter-sample points. The advantage of this approach is that the feedback controller $\boldsymbol{C}_2[z]$ is completely independent of the repetitive controller. Thus, stability robustness is guaranteed by the feedback controller obtained from robust control theory. With this scheme, it becomes possible to construct the repetitive controller without sacrifice of the feedback characteristics.

4 Applications to visual servo system

In this section, the visual servo problem is considered, in which the camera mounted on the robot manipulator tracks a moving object as shown in Fig. 6. Although the sampling period of vision sensor such as a CCD camera is comparatively slow (over 33 [ms]), the control period of joint servo is fast (less than 1 [ms]). Therefore, multirate controllers have been developed and implemented in the visual servo system (e.g. [13]). In this section, it is assumed that the motion of the object is periodic, and repetitive disturbance rejection control is applied based on the multirate feedback and feedforward approaches developed in section 3.

In order to focus on the dynamical problems of the multirate system, the kinematical problems of the visual servo system are assumed to be simple: the object movement is in two-dimensional plane, and the depth information between the camera and the object z is known.

4.1 Modeling of Visual Servo System

First, the work space position controller is designed in order to control the camera position as shown in Fig. 7 [14]. Because this controller employs the robust disturbance observer (DOB) in the joint space, each joint axis is decoupled. Therefore, if the non-singularity of Jacobian $\boldsymbol{J}_{aco}$ is assured, the transfer function from

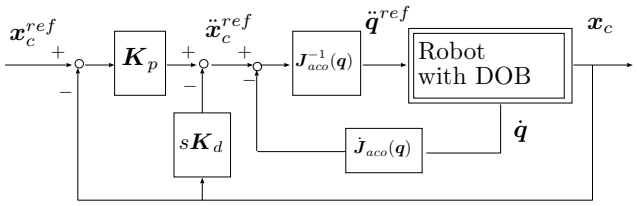

Figure 7: Workspace controller (inner-loop).

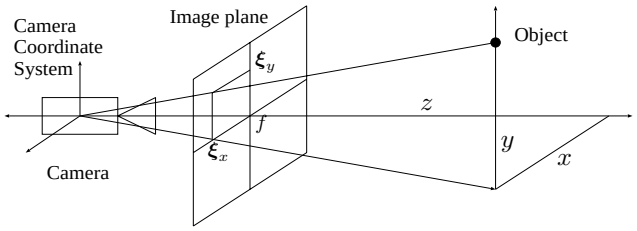

Figure 8: Perspective model

the work space acceleration command $\ddot{\boldsymbol{x}}_c^{ref}$ to the work space position $\boldsymbol{x}_c(=[X_c, Y_c]^T)$ can be regarded as a double integrator system for the frequency region below the cut-off frequency [14]. Letting $\boldsymbol{x}_c^{ref}$ be the control input $\boldsymbol{u}$ of the outer vision loop, the plant is modeled by the analog system (38) because the sampling period of the inner-loop is very short (1 [ms] in this experiment).

$$\boldsymbol{x}_c(s) = \boldsymbol{P}_c(s)\boldsymbol{u}(s), \quad \boldsymbol{P}_c(s) := \frac{K_p}{s^2 + K_d s + K_p}\boldsymbol{I}_2 \qquad (38)$$

In Fig. 7, the parameters of the position controller are set to $\boldsymbol{K}_p = diag\{100, 100\}$ and $\boldsymbol{K}_d = diag\{20, 20\}$.

Next, the perspective model of the camera is derived. In Fig. 7, the object position (x, y) on the camera coordinate system is determined only by the relative position between the camera position $\boldsymbol{x}_c$ and object position $\boldsymbol{x}_o$. Therefore, the following model is obtained because (x, y) is mapped to the feature point $\boldsymbol{\xi}$ on the image plane, as shown in Fig. 8 [13].

$$\boldsymbol{\xi} = \frac{f}{z}\begin{bmatrix} x \\ y \end{bmatrix} = \frac{f}{z}\begin{bmatrix} \cos\theta & \sin\theta \\ -\sin\theta & \cos\theta \end{bmatrix}\begin{bmatrix} X_o - X_c \\ Y_o - Y_c \end{bmatrix} \qquad (39)$$

Here f is the focus distance, z is the distance between the object and camera in the Z-axis direction, and $\theta := q_1 + q_2$. Equation (39) is described by $\boldsymbol{\xi} = \iota(\theta)(\boldsymbol{x}_o - \boldsymbol{x}_c) = \iota(\theta)\boldsymbol{x}_e$.

Fig. 9 shows the proposed control system. In this experiment, the desired feature $\boldsymbol{\xi}^{ref}$ is set to zero because the camera is controlled to be positioned just below the object. The movement of the object can be modeled as the output disturbance $\boldsymbol{x}_o$. Therefore, the proposed method can achieve high tracking performance because the periodic motion can be rejected by the proposed PDR. Moreover, the control system of Fig. 9 is linearized and diagonalized by the inverse transformation $\iota^{-1}(\theta)$ of (39)[2]. Thus, the controllers can be designed

[2]In case of the setup of Fig. 9, $\iota^{-1}(\theta)$ is easily obtained from the inverse matrix of (39). In general case, it can be calculated from the inverse Jacobian.

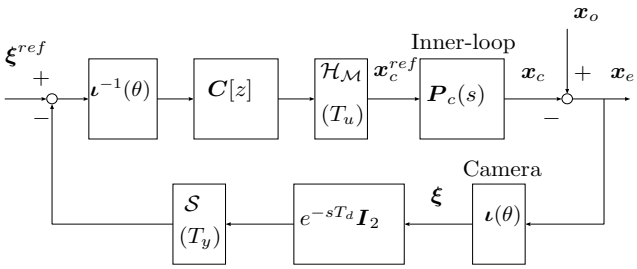

Figure 9: Visual servo system.

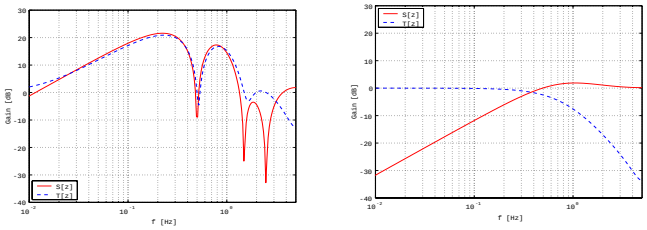

(a) Feedback (b) Feedforward

Figure 10: Frequency responses ($S[z]$ and $T[z]$).

independently in the x and y axes. The sampling period of the image and the control period of the position command $\boldsymbol{x}_c^{ref}$ are set to $T_y = 100$ [ms] and $T_u = 25$ [ms], respectively. Because the input multiplicity is $N = 4$ and the order of plant (38) is $n = 2$, perfect disturbance rejection is assured at $2(= N/n)$ intersample points. The time delay caused by image processing is $T_d = 100$ [ms].

4.2 Simulation and Experimental Results

In the experiments, a two-link direct drive robot is utilized, and a personal computer is used both for joint servo control and image processing. The repetitive disturbance is modeled for $k =$ 1st, 3rd, and 5th order. The period of the object's movement is $T_0 = 0.5$[s].

Fig. 10 shows the sensitivity and complementary sensitivity functions $S[z]$ and $T[z]$ both of the feedback (Fig. 3) and the feedforward (Fig. 5) control systems. Fig. 10(a) indicates the disadvantages of the feedback repetitive controller, where the closed-loop characteristics worsen and it becomes difficult to assure stability robustness. On the other hand, in the proposed feedforward repetitive control (Fig. 5), the closed-loop characteristics depend only on $\boldsymbol{C}_2[z]$ which does not need to have the internal model of repetitive disturbance. Therefore, the feedback characteristics are better than those of the feedback approach.

Fig. 11 shows the simulated results of position error $X_o - X_c$ for circular movement of the object. As shown in Fig. 11(a), the position error of the feedforward controller converges quickly after the switching action at

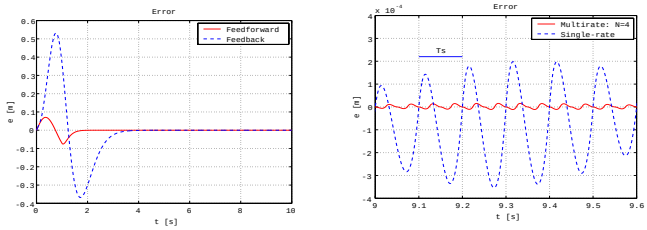

(a) Feedforward vs. Feedback

(b) Multirate vs. Single-rate

Figure 11: Position Error $X_o - X_c$ (simulation).

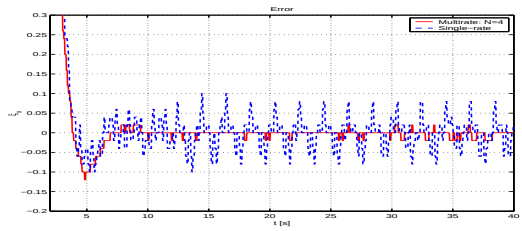

(a) Error in ξ_x

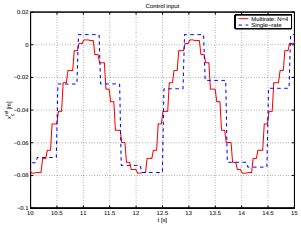

(b) Control input X_c^{ref}

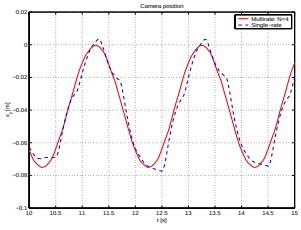

(c) Camera position X_c

Figure 12: Experimental results ($T_y = 400$ [ms], $N = 4$)

.

$t_0 = 1.0$[s], while that of the feedback controller has large transient errors. In the steady state, the errors of the position and velocity become zero at every $T_y/2$ with the proposed controllers as shown in Fig. 11(b). The intersample position error of the proposed multirate method is much smaller than that of the single-rate controller.

The experimental results are shown in Fig. 12. In these experiments, the image is detected at every 100 [ms]. In order to display the intersample response, the sampling period is set to $T_y = 400$ [ms] in the controller. Fig. 12(a) shows that the tracking error of the proposed multirate controller is much smaller than that of the single-rate controller. Moreover, as shown in Fig. 12(b) and (c), the camera position is very smooth because the multirate controller generates the intersample position reference based on the disturbance model. Note that the amplitude and phase of the target movement are assumed to be unknown, and the information is estimated by the observer.

5 Conclusion

In this paper, the repetitive disturbance rejection controllers were applied to the visual servo system of robot manipulator based on the multirate sampling control. Because the proposed control system assured the perfect disturbance rejection at M intersample points, the control system achieved high tracking performance. Moreover, the time delay for image processing was compensated by the developed observer. Next, the novel scheme of repetitive control was proposed based on the open-loop estimation and switching function, which enabled to reject periodical disturbance without any sacrifice of the feedback characteristics. The advantages of these approaches were demonstrated through simulations and experiments using two-link direct drive robot.

References

[1] M. Araki, "Recent developments in digital control theory," in *12th IFAC World Congress*, vol. 9, pp. 251–260, July 1993.

[2] H. Fujimoto, *General Framework of Multirate Sampling Control and Applications to Motion Control Systems*. PhD thesis, The University of Tokyo, December 2000.

[3] H. Fujimoto, Y. Hori, and A. Kawamura, "Perfect tracking control based on multirate feedforward control with generalized sampling periods," *IEEE Trans. Industrial Electronics*, vol. 48, no. 3, pp. 636–644, 2001.

[4] H. Fujimoto, Y. Hori, T. Yamaguchi, and S. Nakagawa, "Proposal of perfect tracking and perfect disturbance rejection control by multirate sampling and applications to hard disk drive control," in *Conf. Decision Contr.*, pp. 5277–5282, 1999.

[5] P. P. Khargonekar, K. Poolla, and A. Tannenbaum, "Robust control of linear time-invariant plants using periodic compensation," *IEEE Trans. Automat. Contr.*, vol. 30, no. 11, pp. 1088–1096, 1985.

[6] J. S. Shamma and M. A. Dahleh, "Time-varying versus time-invariant compensation for rejection of persistent bounded disturbances and robust stabilization," *IEEE Trans. Automat. Contr.*, vol. 36, no. 7, pp. 838–847, 1991.

[7] H. Fujimoto, A. Kawamura, and M. Tomizuka, "Generalized digital redesign method for linear feedback system based on N-delay control," *IEEE/ASME Trans. Mechatronics*, vol. 4, no. 2, pp. 101–109, 1999.

[8] T. Chen and B. Francis, *Optimal Sampled-Data Control Systems*. Springer, 1995.

[9] M. Araki and T. Hagiwara, "Pole assignment by multirate-data output feedback," *Int. J. Control*, vol. 44, no. 6, pp. 1661–1673, 1986.

[10] H. Fujimoto and Y. Hori, "Vibration suppression and optimal repetitive disturbance rejection control in semi-nyquist frequency region using multirate sampling control," in *Conf. Decision Contr.*, pp. 691–700, 2000.

[11] G. F. Franklin and J. D. Powell, *Digital Control of Dynamic Systems*. Addison-Wesley Publishing Company, 1980.

[12] C. Smith, K. Takeuchi, and M. Tomizuka, "Cost effective repetitive controllers for data storage devices," in *14th IFAC World Congress*, vol. B, pp. 407–412, July 1999.

[13] K. Hashimoto and H. Kimura, "Visual servoing with nonlinear observer," *IEEE Int. Conf. Robotics and Automation*, pp. 484–489, 1995.

[14] T. Murakami, N. Oda, Y. Miyasaka, and K.Ohnishi, "A motion control strategy based on equivalent mass matrix in multidegree-of-freedom manipulator," *IEEE Trans. Industrial Electronics*, vol. 42, no. 2, pp. 259–265, 1995.